(Received 10 June 2026, Accepted 6 July 2026, Scheduled 25 July 2026)

Doppler-Aware Robust Quantized RIS Phase Optimization for Physical Layer Security in 6G Vehicular Networks under Imperfect CSI

Ravi Patel* and Atul Patel

Faculty of Computer Science and Applications (CMPICA)
Charotar University of Science and Technology (CHARUSAT), Anand, Gujarat, India

ABSTRACT: Reconfigurable Intelligent Surfaces (RISs) can support physical-layer security in sixth-generation (6G) vehicular networks by reconfiguring the wireless channel. However, RIS-assisted vehicular links are affected by Doppler-induced channel aging, imperfect channel state information (CSI), feedback delay, and finite-resolution phase control. This paper develops a bounded-uncertainty Doppler-Aware Robust Quantized Alternating Optimization (DA-RQ-AO) framework for secure RIS-assisted 6G vehicular communication under imperfect and delayed CSI. The system includes a multi-antenna transmitter, a legitimate receiver, a passive eavesdropper, and a roadside RIS. A robustness-aware secrecy-rate surrogate is formulated by jointly optimizing the transmit beamformer and quantized RIS phase shifts under power, unit-modulus, CSI-uncertainty, and discrete-phase constraints. The non-convex problem is addressed through alternating optimization, where the beamformer is updated using a conservative generalized eigenvector-based solution, and the RIS phase vector is refined using an explicitly derived chain-rule-based phase-gradient update followed by finite-resolution quantization with an acceptance safeguard. Numerical results show improved secrecy rate and lower secrecy outage probability than no-RIS, random-RIS, Q-AO, and robust AO benchmarks. For $N = 64$, the proposed scheme improves secrecy rate by 118.8% over no-RIS and 73.8% over random RIS, while 2-bit RIS control shows only 5.94% loss relative to continuous phase control.

1. INTRODUCTION

Vehicle-to-everything (V2X) communication is expected to become an important application domain of sixth-generation (6G) wireless networks, supporting connected and autonomous vehicles, intelligent transportation systems, cooperative driving, remote control, and safety-critical information exchange. Compared with conventional vehicular communication technologies, 6G-enabled V2X networks are expected to require higher data rates, ultra-reliable, low-latency communication, massive connectivity, and intelligent adaptation to highly dynamic traffic environments [1]. These requirements are difficult to satisfy in practical vehicular scenarios because wireless links are strongly affected by high mobility, rapid channel variations, Doppler shifts, blockage, multipath propagation, and frequent topology changes. In addition to reliability and latency, security remains a major concern because the broadcast nature of wireless propagation exposes vehicular links to eavesdropping.

Traditional cryptographic mechanisms are widely used to secure vehicular networks, but they mainly operate at the upper protocol layers and may introduce additional computational and signaling overhead. Future 6G vehicular systems will involve a large number of latency-sensitive and resource-constrained devices, where lightweight and complementary security mechanisms are required. Physical Layer Security (PLS) has therefore attracted attention as a complementary security approach for 6G networks. PLS exploits the randomness and spatial characteristics of wireless channels to improve the secrecy performance against unauthorized receivers without relying solely on computational hardness [2]. However, achieving reliable PLS in vehicular communication is challenging because high-speed mobility leads to time-varying channels, imperfect channel state information (CSI), and rapid degradation of beam alignment between legitimate users and eavesdroppers.

Reconfigurable Intelligent Surfaces (RISs), also known as Intelligent Reflecting Surfaces (IRSs), have emerged as a key enabling technology for 6G wireless systems. An RIS consists of a large number of nearly passive reflecting elements whose phase responses can be electronically controlled to reconfigure a wireless propagation environment. By adjusting the phase shifts of RIS elements, reflected signals can be constructively combined at legitimate receivers and weakened toward unauthorized receivers. RIS technology has been widely studied for improving coverage, spectrum efficiency, energy efficiency, beamforming gain, and physical layer security in future wireless networks [3, 4]. In vehicular environments, roadside RIS deployment is attractive because it can help mitigate blockage, extend coverage, and improve link reliability for vehicle-to-everything (V2X) communications [5]. Nevertheless, many RIS-assisted vehicular communication studies primarily focus on throughput, coverage, or scheduling, whereas

* Corresponding author: Ravi Patel (ravipatel.mca@charusat.ac.in).

secrecy-oriented designs under mobility, CSI, and hardware constraints remain less explored.

RIS-assisted PLS has been investigated in several wireless scenarios, including multi-user systems, Non-Orthogonal Multiple Access (NOMA) networks, wireless-powered communication systems, and Multiple-Input Multiple-Output (MIMO) secure communication models. Existing studies have shown that joint transmit beamforming and RIS phase-shift optimization can improve the secrecy rate and reduce information leakage toward eavesdroppers [6–9]. Robust beamforming schemes under imperfect CSI and discrete RIS phase-shift constraints have also been proposed for secure IRS-aided communication systems [10]. Recent surveys have further indicated that channel state information (CSI) acquisition, RIS hardware impairments, phase quantization, mobility, secrecy outage probability, and computational complexity are important open issues for practical RIS-assisted PLS deployment in next-generation wireless networks [11–13]. However, these studies are generally developed for static or quasi-static wireless systems and do not fully capture Doppler-induced channel aging and high-speed mobility in 6G vehicular networks.

RIS-assisted secure vehicular communication has also received initial attention. Makarfi et al. investigated physical layer security in vehicular networks with reconfigurable intelligent surfaces, demonstrating the potential of RIS deployment for secure vehicular links [14]. A preliminary conference version of this work [15] introduced an RIS-assisted PLS framework for 6G vehicular networks, where transmit beamforming and RIS phase shifts were jointly optimized using an alternating optimization approach to improve the secrecy rate under vehicular mobility. However, that work assumed idealized CSI availability and continuous RIS phase control. Such assumptions may not hold in practical 6G vehicular deployments because the CSI becomes outdated under high-speed mobility; feedback delay causes channel aging; and real RIS hardware supports only finite-resolution phase shifts. Therefore, a more practical secrecy optimization framework is required to jointly consider Doppler mobility, imperfect CSI, CSI feedback delay, and quantized RIS phase control.

Motivated by these limitations, this study develops a bounded-uncertainty Doppler-aware robust quantized Alternating Optimization (DA-RQ-AO) framework for RIS-assisted physical-layer security in 6G vehicular networks with imperfect and delayed CSI. The considered system consists of a multi-antenna vehicular transmitter, a legitimate vehicular receiver, a passive eavesdropper, and a roadside RIS. The objective is to improve the secrecy performance by jointly optimizing the transmit beamforming vector and RIS phase-shift configuration under CSI uncertainty, feedback delay, Doppler-induced channel aging, passive-Eve uncertainty, and finite-resolution RIS phase quantization. The novelty is not claimed as a new globally optimal optimization class; rather, it lies in integrating these practical non-idealities into one reproducible vehicular PLS framework with a conservative secrecy surrogate, explicit RIS phase-gradient derivation, quantized update safeguard, and multi-metric reliability evaluation.

The main contributions of this paper are as follows.

1. A practical RIS-assisted 6G vehicular PLS model is developed by incorporating Doppler-induced channel aging, imperfect and delayed CSI, passive-Eve bounded uncertainty, and finite-resolution RIS phase control into the secrecy-rate optimization framework.

2. A bounded-uncertainty robustness-aware secrecy-rate surrogate is formulated by conservatively lower-bounding Bob's Signal-to-Noise Ratio (SNR) and upper-bounding Eve's SNR, clarifying the practical robust-design interpretation without claiming a globally solved min-max optimum.

3. A DA-RQ-AO algorithm is developed to jointly update the transmit beamformer and RIS phases. The beamforming step uses a conservative generalized eigenvector-based update, while the RIS step is supported by an explicit chain-rule-based phase-gradient derivation, continuous projection, finite-resolution quantization, and an acceptance safeguard.

4. The impact of RIS element scaling, vehicle speed, CSI error variance, CSI feedback delay, and 1-bit/2-bit/3-bit RIS phase resolution is evaluated using average secrecy rate and secrecy outage probability under a Monte Carlo simulation protocol.

5. The convergence behavior, computational complexity, and benchmark scope are discussed to clarify that the proposed method provides numerical stabilization of feasible iterates under the adopted surrogate objective, rather than a guarantee of global optimality for the original mixed-integer non-convex problem.

The numerical evaluation shows that the proposed DA-RQ-AO scheme provides higher secrecy performance than the no-RIS, random-RIS, quantized AO, and non-Doppler-aware robust AO benchmark schemes under imperfect CSI and high-mobility conditions. The results also indicate that low-resolution RIS phase control, particularly 2-bit quantization, can achieve limited degradation relative to continuous phase control while reducing the hardware complexity. These findings suggest that RIS-assisted PLS becomes more practical for 6G vehicular networks when Doppler mobility, CSI aging, and RIS quantization are jointly considered.

The remainder of this paper is organized as follows. Section 2 reviews the related work and identifies the research gap. Section 3 presents the system and channel model. Section 4 formulates the secrecy-rate maximization problem under imperfect CSI and quantized RIS constraints. Section 5 describes the proposed DA-RQ-AO algorithm. Section 6 presents the numerical results and performance discussion. Finally, Section 7 concludes the paper and outlines the future research directions.

2. RELATED WORK AND RESEARCH GAP

This section reviews the literature related to RIS-assisted physical layer security in 6G vehicular networks. The discussion is organized around 6G-V2X communication, RIS-assisted wireless and vehicular communication, RIS-enabled physical layer

security, imperfect CSI and quantized phase control, and the specific research gap addressed in this study.

2.1. 6G-V2X Communication and Vehicular Security Requirements

Vehicle-to-everything (V2X) communication is expected to be an important application area for 6G wireless networks because future intelligent transportation systems require reliable, low-latency, high-capacity, and adaptive communication links. Noor-A-Rahim et al. [1] presented a comprehensive overview of 6G-enabled V2X communication and discussed enabling technologies, challenges, and opportunities for future vehicular networks. Their study highlighted that connected and autonomous vehicles require communication architectures capable of supporting high mobility, strict latency constraints, and dynamic traffic conditions. Because vehicular messages are transmitted over open wireless channels, unauthorized receivers may intercept safety, control, or identity-related information. Therefore, physical layer security has become a relevant complementary security mechanism for 6G vehicular communication.

Mitev et al. [2] discussed the role of physical layer security in 6G systems and explained how wireless-channel characteristics can be exploited to improve secrecy beyond conventional cryptographic mechanisms. This direction is particularly relevant to vehicular networks, where low latency and high mobility may limit the exclusive use of upper-layer security techniques. However, applying physical layer security in vehicular environments remains challenging because the channel state information becomes rapidly outdated, and the quality difference between the legitimate and eavesdropping links may change quickly owing to mobility.

2.2. RIS-Assisted Wireless and Vehicular Communication

RISs have emerged as a promising 6G technology for controlling the wireless propagation environment. Pan et al. [3] reviewed the principles, applications, and research directions of RIS-assisted 6G systems. Wu and Zhang [4] developed a foundational joint active and passive beamforming framework for RIS-assisted wireless networks and demonstrated that optimized RIS phase shifts can improve communication performance.

The deployment of RISs is also attractive in vehicular environments, where direct communication links may be blocked by buildings, vehicles, and roadside objects. Zhu et al. [5] surveyed RIS applications in 6G vehicular communications and identified the potential of RIS for enhancing coverage, mitigating blockage, supporting localization, and improving secure communication. Al-Hilo et al. [16] studied RIS-enabled vehicular communication through joint user scheduling and passive beamforming, and showed that RIS deployment can improve communication performance in dynamic vehicular scenarios. Recent RIS optimization work has also considered phase design for 6G-oriented wireless systems, although the focus is on SWIPT rather than vehicular physical-layer security [17]. Despite these advances, many RIS-assisted vehicular studies have focused mainly on throughput, coverage, scheduling, and resource allocation. Secrecy-oriented RIS designs under mobility, CSI uncertainty, and hardware phase-resolution constraints remain comparatively less explored.

2.3. RIS-Assisted Physical Layer Security

RIS-assisted physical layer security has been widely investigated because RIS phase control can enhance legitimate links while reducing signal leakage to eavesdroppers. Yu et al. [6] proposed a robust and secure IRS-assisted wireless communication framework that jointly optimizes transmit beamforming, artificial noise, and IRS phase shifts under imperfect eavesdropper CSI. Jiang et al. [7] studied IRS-assisted secure wireless communication with multiple transmitting and receiving antennas and considered both continuous and discrete IRS phase shifts. Zhang et al. [8] investigated RIS-aided NOMA 6G networks and showed that joint beamforming, power allocation, and artificial noise can improve secrecy performance. Cao et al. [9] analyzed IRS-aided wireless-powered communication systems and considered secrecy-related reliability metrics such as connection outage probability, secrecy outage probability, and effective secrecy throughput.

Recent surveys further confirm the importance of RIS-assisted PLS and identify several practical challenges. Khalid et al. [11] reviewed RIS-based physical layer security for 6G-IoT systems and discussed issues related to channel estimation, optimization complexity, and RIS modeling. Kaur et al. [12] surveyed RIS-assisted physical layer security for next-generation wireless communications and highlighted open problems such as channel state information (CSI) availability, hardware impairments, mobility, multiple eavesdroppers, and quality-of-service-aware security. Khoshafa et al. [13] reviewed RIS-assisted PLS in RF and optical wireless communication systems and emphasized the secrecy performance analysis, optimization methods, and implementation challenges.

2.4. Imperfect CSI, Robust Optimization, and Quantized RIS Phase Control

Perfect CSI is commonly assumed in many RIS-assisted communication studies; however, this assumption is difficult to satisfy in practical 6G vehicular networks. Owing to high-speed mobility, the CSI estimation and feedback may become outdated before the RIS phase shifts are applied. Shen et al. [10] studied robust beamforming for IRS-aided secure communication systems under complete imperfect CSI. Their work considered uncertainty in both legitimate and eavesdropping channels and optimized the transmit beamforming with discrete IRS phase shifts. Yu et al. [6] also considered imperfect CSI in robust IRS-assisted secure communication. These studies show that robust optimization can improve the secrecy performance under channel uncertainty. However, they did not explicitly address Doppler-induced CSI aging in vehicular networks.

Another practical issue is RIS phase quantization. Ideal continuous phase shifts are difficult to implement in low-cost RIS hardware, whereas practical RIS elements usually support

TABLE 1. Comparison of representative RIS-assisted communication and security studies with the proposed work.

Reference	Main focus	System scenario	Imperfect CSI	Quantized RIS	Mobility/ Doppler	Main limitation for vehicular PLS
Wu and Zhang [4]	Joint active and passive beamforming	General RIS-assisted wireless network	No	No	No	Does not consider secrecy, vehicular mobility, or CSI aging
Pan et al. [3]	RIS principles and 6G applications	General 6G RIS systems	General	General	No	Does not provide a vehicular PLS optimization framework
Zhu et al. [5]	RIS in 6G vehicular communication	Vehicular communication	General	Limited	Yes	Security optimization under imperfect CSI and quantization remains open
Yu et al. [6]	Robust IRS-assisted secure communication	multi-user secure wireless system	Yes	No	No	Does not consider vehicular Doppler mobility or quantized RIS
Jiang et al. [7]	IRS-assisted secrecy-rate maximization	MIMO secure communication	No	Yes	No	No vehicular mobility or CSI aging analysis
Shen et al. [10]	Robust IRS secure beamforming	Secure wireless communication	Yes	Yes	No	Does not address Doppler-aware vehicular channels
Patel and Patel [15]	RIS-assisted vehicular PLS	6G vehicular network	No	No	Yes	Does not consider imperfect CSI, CSI delay, quantized RIS, or SOP
Proposed work	**DA-RQ-AO for RIS-assisted vehicular PLS**	**6G vehicular network**	**Yes**	**Yes**	**Yes**	**Jointly considers Doppler mobility, imperfect CSI, feedback delay, quantized RIS, secrecy rate, SOP, and convergence**

finite-resolution phase states such as 1-bit, 2-bit, or 3-bit configurations. Jiang et al. [7] considered discrete IRS phase-shift design for secure communication, and Shen et al. [10] included discrete IRS phase control under imperfect CSI. These studies show that quantized RIS phase design is important for practical deployment. However, the joint effect of phase quantization, imperfect CSI, feedback delay, and high-speed Doppler mobility on the secrecy rate and secrecy outage probability has not been sufficiently investigated for 6G vehicular PLS.

2.5. Research Gap and Motivation

The existing literature indicates that RIS technology can improve wireless communication performance and that RIS-assisted PLS can enhance secrecy in several static or quasi-static communication scenarios. However, important limitations remain when these methods are applied to 6G vehicular networks. First, many RIS-assisted PLS studies assume static or slowly varying channels, which do not capture Doppler-induced channel variation in high-mobility vehicular communication. Second, perfect or nearly perfect CSI is frequently assumed, although the CSI feedback delay causes channel aging in practical systems. Third, continuous RIS phase shifts are often used as an ideal benchmark, whereas practical RIS hardware supports only finite-resolution phase control. Fourth, several studies focus mainly on the average secrecy rate, whereas the secrecy outage probability is also needed to evaluate secure communication reliability.

A preliminary conference version of this work [15] introduced an RIS-assisted physical layer security framework for 6G vehicular networks and reported secrecy-rate improvement through joint transmit beamforming and RIS phase optimization. However, that study assumed ideal CSI availability and did not explicitly address quantized RIS phase shifts, imperfect CSI, CSI feedback delay, or secrecy outage probability. These limitations motivate the present study.

Table 1 summarizes representative RIS-assisted communication and security studies and highlights the specific gap addressed by the proposed DA-RQ-AO framework.

Based on the above discussion, the main research gap can be stated as follows: existing RIS-assisted PLS frameworks have studied several important aspects, such as robust beamforming, discrete RIS phase shifts, and secrecy-rate maximization, but they have not sufficiently integrated Doppler-induced vehicular channel aging, imperfect and delayed CSI, passive-Eve bounded uncertainty, finite-resolution RIS phase control, secrecy outage reliability, convergence behavior, and

implementation-aware complexity within a single 6G vehicular security model. This study addresses this gap through the proposed DA-RQ-AO framework. The contribution is therefore positioned as a practical integration and rigorous adaptation of RIS-assisted secrecy optimization to Doppler-aged vehicular channels, rather than as a claim of globally optimal robust min-max optimization.

3. SYSTEM AND CHANNEL MODEL

This section presents the RIS-assisted secure vehicular communication model considered in this study. The system consists of a multi-antenna legitimate transmitter Alice, a single-antenna legitimate vehicular receiver Bob, a single-antenna passive eavesdropper Eve, and a roadside RIS equipped with N reflecting elements. Alice is equipped with M transmitting antennas and sends confidential information to Bob in the presence of Eve. The RIS is deployed near the roadside infrastructure to assist the wireless propagation link by adjusting the phase shifts of its reflecting elements.

3.1. Signal Transmission Model

Let $s(t)$ denote the confidential information symbol transmitted by Alice at time t, where $\mathbb{E}\{|s(t)|^2\} = 1$. Alice applies the transmit beamforming vector $\mathbf{w}(t) \in \mathbb{C}^{M\times 1}$, and the transmitted signal is expressed as

$$\mathbf{x}(t) = \mathbf{w}(t)s(t), \tag{1}$$

subject to the transmit power constraint

$$\|\mathbf{w}(t)\|^2 \le P_{\max}. \tag{2}$$

The direct channels from Alice to Bob and Eve are denoted by $\mathbf{h}_{AB}(t) \in \mathbb{C}^{M\times 1}$ and $\mathbf{h}_{AE}(t) \in \mathbb{C}^{M\times 1}$, respectively. The Alice-to-RIS channel is denoted as $\mathbf{G}_{AR}(t) \in \mathbb{C}^{N\times M}$. The RIS-to-Bob and RIS-to-Eve channels are denoted by $\mathbf{h}_{RB}(t) \in \mathbb{C}^{N\times 1}$ and $\mathbf{h}_{RE}(t) \in \mathbb{C}^{N\times 1}$, respectively.

The RIS phase-shift matrix with b-bit phase resolution is defined as

$$\mathbf{\Theta}_b(t) = \mathrm{diag}\left\{e^{j\theta_1^{(b)}(t)}, e^{j\theta_2^{(b)}(t)}, \ldots, e^{j\theta_N^{(b)}(t)}\right\}, \tag{3}$$

where the unit reflection amplitude is assumed for each RIS element. For a practical b-bit RIS, the available phase set is as follows:

$$\mathcal{F}_b = \left\{ \frac{2\pi q}{2^b} \,\middle|\, q = 0, 1, \ldots, 2^b - 1 \right\}. \tag{4}$$

Let $\theta_n(t)$ denote the continuous phase value prior to quantization. The nearest quantized phase index is obtained as follows:

$$q_n^\star(t) = \arg \min_{q\in\{0,1,\ldots,2^b-1\}} \left| e^{j\theta_n(t)} - e^{j\frac{2\pi q}{2^b}} \right|, \tag{5}$$

and the corresponding quantized phase is

$$\theta_n^{(b)}(t) = \frac{2\pi q_n^\star(t)}{2^b}. \tag{6}$$

This quantization form maps each continuous phase to the nearest finite-resolution RIS phase state and avoids ambiguity near the 0 and 2π phase boundaries.

The equivalent Alice-Bob channel is given by

$$\mathbf{h}_{B,\mathrm{eff}}^H(t) = \mathbf{h}_{AB}^H(t) + \mathbf{h}_{RB}^H(t)\mathbf{\Theta}_b(t)\mathbf{G}_{AR}(t), \tag{7}$$

and the equivalent Alice-Eve channel is

$$\mathbf{h}_{E,\mathrm{eff}}^H(t) = \mathbf{h}_{AE}^H(t) + \mathbf{h}_{RE}^H(t)\mathbf{\Theta}_b(t)\mathbf{G}_{AR}(t). \tag{8}$$

Both $\mathbf{h}_{B,\mathrm{eff}}^H(t)$ and $\mathbf{h}_{E,\mathrm{eff}}^H(t)$ have dimension $1 \times M$, which is consistent with the transmit beamforming vector $\mathbf{w}(t)$.

The received signals at Bob and Eve are respectively written as

$$y_B(t) = \mathbf{h}_{B,\mathrm{eff}}^H(t)\mathbf{w}(t)s(t) + n_B(t), \tag{9}$$

and

$$y_E(t) = \mathbf{h}_{E,\mathrm{eff}}^H(t)\mathbf{w}(t)s(t) + n_E(t), \tag{10}$$

where $n_B(t) \sim \mathcal{CN}(0, \sigma_B^2)$ and $n_E(t) \sim \mathcal{CN}(0, \sigma_E^2)$ denote the additive white Gaussian noise at Bob and Eve, respectively. Therefore, the instantaneous SNRs are

$$\gamma_B(t) = \frac{\left|\mathbf{h}_{B,\mathrm{eff}}^H(t)\mathbf{w}(t)\right|^2}{\sigma_B^2}, \tag{11}$$

and

$$\gamma_E(t) = \frac{\left|\mathbf{h}_{E,\mathrm{eff}}^H(t)\mathbf{w}(t)\right|^2}{\sigma_E^2}. \tag{12}$$

3.2. Rician Vehicular Channel Model

For a generic wireless link between nodes i and j, the large-scale channel gain is modeled as

$$\beta_{ij}(d_{ij}) = \beta_0 \left(\frac{d_{ij}}{d_0}\right)^{-\alpha_{ij}}, \tag{13}$$

where d_{ij} is the link distance, d_0 the reference distance, β_0 the channel gain at d_0, and α_{ij} the path-loss exponent.

The corresponding small-scale fading channel is modeled using Rician fading as

$$\mathbf{H}_{ij}(t) = \sqrt{\beta_{ij}(d_{ij})}\left(\sqrt{\frac{K_{ij}}{K_{ij}+1}}\mathbf{H}_{ij}^{\mathrm{LoS}}(t) + \sqrt{\frac{1}{K_{ij}+1}}\mathbf{H}_{ij}^{\mathrm{NLoS}}(t)\right), \tag{14}$$

where K_{ij} is the Rician factor, $\mathbf{H}_{ij}^{\mathrm{LoS}}(t)$ the deterministic line-of-sight component, and $\mathbf{H}_{ij}^{\mathrm{NLoS}}(t)$ the non-line-of-sight scattering component. Depending on the considered link, $\mathbf{H}_{ij}(t)$ represents either the channel vector or matrix. This model is applied to the direct Alice-Bob and Alice-Eve links, Alice-RIS link, and RIS-Bob/RIS-Eve links.

3.3. Doppler-Aware Channel Aging Model

Let v denote the relative vehicle speed, f_c the carrier frequency, and c the light speed. The maximum Doppler frequency is expressed as

$$f_D = \frac{v f_c}{c}, \tag{15}$$

where v is expressed in m/s when the Doppler frequency is evaluated. For a propagation path with angle ψ relative to the direction of motion, the path-dependent Doppler shift is expressed as

$$f_D(\psi) = \frac{v f_c}{c}\cos(\psi). \tag{16}$$

For any time-varying channel $\mathbf{X}(t)$, the channel aging relation is modeled as follows:

$$\mathbf{X}(t) = \rho_X(\tau)\mathbf{X}(t-\tau) + \sqrt{1-|\rho_X(\tau)|^2}\mathbf{E}_X(t), \tag{17}$$

where $\mathbf{X}(t) \in \{\mathbf{h}_{AB}(t), \mathbf{h}_{AE}(t), \mathbf{h}_{RB}(t), \mathbf{h}_{RE}(t), \mathbf{G}_{AR}(t)\}$, τ is the CSI feedback delay, and $\mathbf{E}_X(t)$ is an independent innovation term with the same dimension as $\mathbf{X}(t)$. Following the commonly used Doppler/Jakes temporal correlation model for time-varying wireless channels, the temporal correlation coefficient is modeled as follows:

$$\rho_X(\tau) = J_0(2\pi f_{D,X}\tau), \tag{18}$$

where $J_0(\cdot)$ is the zeroth-order Bessel function of the first kind, and $f_{D,X}$ denotes the Doppler frequency associated with channel $\mathbf{X}(t)$ [18]. A larger vehicle speed or feedback delay reduces the correlation between the available CSI and the actual channel, causing phase misalignment in RIS-assisted transmission.

In the proposed framework, Doppler information is not used only as a post-processing parameter. It enters the optimization pipeline through the temporal correlation coefficient $\rho_X(\tau)$ in (17), the delayed CSI available for optimization, and the Doppler-aware uncertainty radius in (29). These quantities affect the robust covariance approximation used in the beamforming update and the delayed effective scalar channels used in the RIS phase-gradient update. Therefore, the term Doppler-aware refers to the use of mobility-dependent channel aging and uncertainty enlargement during the transmit beamforming and RIS phase-optimization steps.

3.4. Imperfect CSI Model

In practice, the channel used for optimization is an imperfect estimate of the actual channel used. For any channel $\mathbf{X}(t)$, the imperfect CSI model is expressed as

$$\mathbf{X}(t) = \widehat{\mathbf{X}}(t) + \Delta\mathbf{X}(t), \tag{19}$$

where $\widehat{\mathbf{X}}(t)$ is the estimated channel, and $\Delta\mathbf{X}(t)$ is the estimation error. In the simulation model, the vectorized estimation error follows

$$\mathrm{vec}\left(\Delta\mathbf{X}(t)\right) \sim \mathcal{CN}\left(\mathbf{0}, \sigma_e^2\mathbf{I}\right). \tag{20}$$

For robust optimization, the corresponding bounded uncertainty set is defined as

$$\mathcal{U}_X = \left\{\mathbf{X}(t) : \mathbf{X}(t) = \widehat{\mathbf{X}}(t) + \Delta\mathbf{X}(t),\ \|\Delta\mathbf{X}(t)\|_F \le \varepsilon_X\right\}, \tag{21}$$

where ε_X denotes the uncertainty radius. Thus, the Gaussian error model is used for numerical channel generation, whereas the bounded set is used in the robust design.

In the considered passive-eavesdropper scenario, Eve does not actively transmit pilot signals to Alice or to the RIS controller. Therefore, the proposed design does not assume exact instantaneous Eve CSI obtained from Eve's pilot transmission. Instead, the eavesdropping channel used for optimization is modeled as a nominal or statistical estimate obtained from long-term channel observations, path-loss information, angular information, radio-environment knowledge, or location-assisted side information. The mismatch between this nominal estimate and the actual passive Eve channel is captured by the uncertainty term $\Delta\mathbf{h}_{E,\tau}(t)$ and the uncertainty radius $\varepsilon_E(t)$.

When reliable nominal information about Eve is limited, the uncertainty radius can be enlarged to represent a more conservative eavesdropping region. In this case, the Eve SNR upper bound in (31) acts as a worst-case surrogate within the assumed bounded uncertainty set. This treatment does not imply that the exact passive Eve channel is known; rather, it provides a conservative design against channel mismatch around the assumed nominal eavesdropping direction or region. Fully unknown Eve locations, multiple hidden passive eavesdroppers, or distributionally robust modeling without nominal Eve-side information require separate stochastic-geometry or environment-mapping formulations and are left as future extensions.

Let $\widehat{\mathbf{X}}_\tau(t) \triangleq \widehat{\mathbf{X}}(t-\tau)$ denote the delayed channel estimate that is available for optimization. The delayed effective estimated Bob channel is then expressed as

$$\widehat{\mathbf{h}}_{B,\tau}^H(t) = \widehat{\mathbf{h}}_{AB,\tau}^H(t) + \widehat{\mathbf{h}}_{RB,\tau}^H(t)\boldsymbol{\Theta}_b(t)\widehat{\mathbf{G}}_{AR,\tau}(t), \tag{22}$$

and the delayed effective estimated Eve channel is

$$\widehat{\mathbf{h}}_{E,\tau}^H(t) = \widehat{\mathbf{h}}_{AE,\tau}^H(t) + \widehat{\mathbf{h}}_{RE,\tau}^H(t)\boldsymbol{\Theta}_b(t)\widehat{\mathbf{G}}_{AR,\tau}(t). \tag{23}$$

4. PROBLEM FORMULATION

This section formulates the robust secrecy-rate maximization problem for the RIS-assisted vehicular physical layer security system. Based on the signal model in Section 3, the transmit beamforming vector and quantized RIS phase-shift matrix are jointly designed under transmit power, CSI uncertainty, Doppler-induced channel aging, and finite-resolution RIS phase constraints.

Using the instantaneous SNRs at Bob and Eve in (11) and (12), the achievable rates of the legitimate and eavesdropping links are expressed as

$$R_B(t) = \log_2\left(1+\gamma_B(t)\right), \quad R_E(t) = \log_2\left(1+\gamma_E(t)\right). \tag{24}$$

Following standard PLS notation [2, 6], the instantaneous secrecy rate is defined as

$$R_s(t) = \left[R_B(t) - R_E(t)\right]^+, \tag{25}$$

where $[x]^+ = \max(x, 0)$. Substituting the SNR expressions gives

$$R_s(t) = \left[\log_2 \left(1 + \frac{\left| \mathbf{h}_{B,\text{eff}}^H(t)\mathbf{w}(t) \right|^2}{\sigma_B^2} \right) - \log_2 \left(1 + \frac{\left| \mathbf{h}_{E,\text{eff}}^H(t)\mathbf{w}(t) \right|^2}{\sigma_E^2} \right) \right]^+. \quad (26)$$

4.1. Robust Secrecy Rate under Imperfect and Delayed CSI

In high-mobility vehicular environments, the channel used for optimization may differ from the actual channel because of estimation error and feedback delay. The effective channels are represented as

$$\begin{aligned} \mathbf{h}_{B,\text{eff}}(t) &= \widehat{\mathbf{h}}_{B,\tau}(t) + \Delta\mathbf{h}_{B,\tau}(t), \\ \mathbf{h}_{E,\text{eff}}(t) &= \widehat{\mathbf{h}}_{E,\tau}(t) + \Delta\mathbf{h}_{E,\tau}(t), \end{aligned} \quad (27)$$

where $\widehat{\mathbf{h}}_{B,\tau}(t)$ and $\widehat{\mathbf{h}}_{E,\tau}(t)$ denote the delayed effective channel estimates, and $\Delta\mathbf{h}_{B,\tau}(t)$ and $\Delta\mathbf{h}_{E,\tau}(t)$ denote the corresponding uncertainty terms.

The effective uncertainty caused by CSI error and Doppler-induced channel aging is modeled as

$$\|\Delta\mathbf{h}_{B,\tau}(t)\|_2 \le \varepsilon_B(t), \qquad \|\Delta\mathbf{h}_{E,\tau}(t)\|_2 \le \varepsilon_E(t), \quad (28)$$

where the Doppler-aware uncertainty radius is expressed as

$$\varepsilon_i(t) = \sqrt{\varepsilon_{i,0}^2 + \eta_i \left(1 - |\rho_i(\tau)|^2 \right)}, \qquad i \in \{B, E\}. \quad (29)$$

Here, $\varepsilon_{i,0}$ is the nominal CSI uncertainty level, η_i a scaling factor associated with the effective channel power, and $\rho_i(\tau)$ the Doppler-dependent temporal correlation coefficient.

Using the triangle inequality and Cauchy-Schwarz inequality, a conservative lower bound for Bob's SNR can be written as

$$\gamma_B^{\text{lb}}(t) = \frac{\left[\left| \widehat{\mathbf{h}}_{B,\tau}^H(t)\mathbf{w}(t) \right| - \varepsilon_B(t)\|\mathbf{w}(t)\|_2 \right]_+^2}{\sigma_B^2}. \quad (30)$$

Similarly, a conservative upper bound for Eve's SNR is given by

$$\gamma_E^{\text{ub}}(t) = \frac{\left[\left| \widehat{\mathbf{h}}_{E,\tau}^H(t)\mathbf{w}(t) \right| + \varepsilon_E(t)\|\mathbf{w}(t)\|_2 \right]^2}{\sigma_E^2}. \quad (31)$$

The robust secrecy rate is therefore defined as

$$R_s^{\text{rob}}(t) = \left[\log_2 \left(1 + \gamma_B^{\text{lb}}(t) \right) - \log_2 \left(1 + \gamma_E^{\text{ub}}(t) \right) \right]^+. \quad (32)$$

This formulation provides a conservative secrecy-rate measure under imperfect and delayed CSI.

It should be noted that the proposed formulation is a bounded-uncertainty robust surrogate rather than a globally solved min-max robust optimization problem. The lower bound for Bob's SNR and the upper bound for Eve's SNR are used to obtain a conservative secrecy-rate objective that can be handled within the alternating optimization procedure. Therefore, the term robust in this work refers to robustness-aware design under bounded CSI uncertainty and Doppler-induced channel aging, rather than a guarantee of global worst-case optimality over all possible channel-error realizations.

4.2. Secrecy Outage Probability and Quantized RIS Constraints

For a target secrecy rate R_{th}, the secrecy outage probability is defined as

$$P_{\text{out}}(R_{\text{th}}) = \Pr\left\{ R_s^{\text{rob}}(t) < R_{\text{th}} \right\}. \quad (33)$$

In Monte Carlo simulations, it is estimated as

$$\widehat{P}_{\text{out}}(R_{\text{th}}) = \frac{1}{L} \sum_{\ell=1}^{L} \mathbf{1}\left\{ R_s^{\text{rob}}(\ell) < R_{\text{th}} \right\}, \quad (34)$$

where L is the number of independent channel realizations, and $\mathbf{1}\{\cdot\}$ is the indicator function.

The RIS reflection vector is defined as

$$\boldsymbol{\phi}_b(t) = \left[e^{j\theta_1^{(b)}(t)}, e^{j\theta_2^{(b)}(t)}, \ldots, e^{j\theta_N^{(b)}(t)} \right]^T. \quad (35)$$

Following practical discrete-phase RIS models [7, 10], each RIS element satisfies the unit-modulus and discrete phase constraints

$$|\phi_n(t)| = 1, \qquad \phi_n(t) \in \mathcal{A}_b, \qquad n = 1, 2, \ldots, N, \quad (36)$$

where

$$\mathcal{A}_b = \left\{ e^{j\frac{2\pi q}{2^b}} \,\middle|\, q = 0, 1, \ldots, 2^b - 1 \right\}. \quad (37)$$

4.3. DA-RQ-AO Optimization Problem

The proposed DA-RQ-AO framework aims to maximize the average robust secrecy rate by jointly optimizing $\mathbf{w}(t)$ and $\boldsymbol{\Theta}_b(t)$. The problem is formulated as follows:

$$\begin{aligned} \mathbf{P1}: \quad & \max_{\mathbf{w}(t), \boldsymbol{\Theta}_b(t)} \quad \mathbb{E}\left\{ R_s^{\text{rob}}(t) \right\} && (38a) \\ \text{s.t.} \quad & \|\mathbf{w}(t)\|^2 \le P_{\max}, && (38b) \\ & \boldsymbol{\Theta}_b(t) = \text{diag}\left(\boldsymbol{\phi}_b(t) \right), && (38c) \\ & \phi_n(t) \in \mathcal{A}_b, \quad n = 1, 2, \ldots, N, && (38d) \\ & \|\Delta\mathbf{h}_{B,\tau}(t)\|_2 \le \varepsilon_B(t), && (38e) \\ & \|\Delta\mathbf{h}_{E,\tau}(t)\|_2 \le \varepsilon_E(t). && (38f) \end{aligned}$$

An outage-aware extension can also be written as

$$P_{\text{out}}(R_{\text{th}}) \le P_{\text{out}}^{\max}, \quad (39)$$

where $P_{\text{out}}^{\max}$ is the maximum tolerable secrecy outage probability. In this study, the outage probability is evaluated as a reliability metric in the numerical results.

TABLE 2. Main system and channel parameters used in the proposed DA-RQ-AO model.

Parameter	Value/Range
Carrier frequency, f_c	28 GHz
Transmit antennas at Alice, M	4
RIS elements, N	$16, 32, 64, 128, 256$
Bob and Eve antennas	Single antenna each
Maximum transmit power, $P_{\max}$	20 dBm
Noise power, σ_B^2, σ_E^2	-90 dBm
Rician factor, K	5 dB
Vehicle speed, v	$30, 60, 90, 120, 150$ km/h
CSI error variance, σ_e^2	$0, 0.02, 0.05, 0.10, 0.15, 0.20$
CSI feedback delay, τ	$0, 1, 2, 5, 10$ ms
RIS phase resolution, b	Continuous, 1-bit, 2-bit, 3-bit
Channel model	Rician fading with path loss
Primary performance metric	Average secrecy rate
Reliability metric	Secrecy outage probability

Problem **P1** is non-convex because the secrecy-rate objective contains a difference of logarithmic functions, the active beamforming vector and passive RIS phase matrix are coupled in the effective channels, and the RIS coefficients are constrained to finite-resolution unit-modulus values. Therefore, a direct exhaustive search over all RIS phase states is computationally expensive for large N. The proposed alternating optimization approach is developed in Section 5 to obtain a feasible low-complexity solution. Table 3 summarizes the main optimization variables and constraints used in the proposed formulation.

5. PROPOSED DA-RQ-AO ALGORITHM

This section presents the proposed Doppler-Aware Robust Quantized Alternating Optimization (DA-RQ-AO) algorithm for solving (38). Because the formulated problem is non-convex, the transmit beamforming vector and the RIS phase-shift vector are updated in an alternating manner. For fixed RIS phases, the transmit beamformer is updated using a robust generalized eigenvector-based solution. For fixed transmit beamforming, the RIS phase vector is updated using a projected gradient step followed by finite-resolution phase quantization.

5.1. Transmit Beamforming Update

For fixed $\boldsymbol{\Theta}_b^{(k)}$, the delayed effective channel estimates of Bob and Eve at the k-th iteration are expressed as

$$\left(\widehat{\mathbf{h}}_{B,\tau}^{(k)}\right)^H = \widehat{\mathbf{h}}_{AB,\tau}^H + \widehat{\mathbf{h}}_{RB,\tau}^H \boldsymbol{\Theta}_b^{(k)} \widehat{\mathbf{G}}_{AR,\tau}, \tag{40}$$

and

$$\left(\widehat{\mathbf{h}}_{E,\tau}^{(k)}\right)^H = \widehat{\mathbf{h}}_{AE,\tau}^H + \widehat{\mathbf{h}}_{RE,\tau}^H \boldsymbol{\Theta}_b^{(k)} \widehat{\mathbf{G}}_{AR,\tau}. \tag{41}$$

TABLE 3. Optimization variables and constraints in the proposed DA-RQ-AO formulation.

Item	Description
$\mathbf{w}(t)$	Transmit beamforming vector at Alice
$\boldsymbol{\Theta}_b(t)$	Quantized RIS phase-shift matrix
$\boldsymbol{\phi}_b(t)$	RIS reflection coefficient vector
$P_{\max}$	Maximum transmit power constraint
$\mathcal{A}_b$	b-bit discrete RIS phase alphabet
$\varepsilon_B(t)$, $\varepsilon_E(t)$	Doppler-aware CSI uncertainty radii
$R_s^{\mathrm{rob}}(t)$	Robust secrecy-rate objective
$P_{\mathrm{out}}(R_{\mathrm{th}})$	Secrecy outage probability metric

The corresponding robust covariance matrices are approximated as

$$\mathbf{R}_B^{(k)} = \Pi_+ \left(\widehat{\mathbf{h}}_{B,\tau}^{(k)} \left(\widehat{\mathbf{h}}_{B,\tau}^{(k)}\right)^H - \left(\varepsilon_B^{(k)}\right)^2 \mathbf{I}_M \right), \tag{42}$$

and

$$\mathbf{R}_E^{(k)} = \widehat{\mathbf{h}}_{E,\tau}^{(k)} \left(\widehat{\mathbf{h}}_{E,\tau}^{(k)}\right)^H + \left(\varepsilon_E^{(k)}\right)^2 \mathbf{I}_M, \tag{43}$$

where $\Pi_+(\cdot)$ denotes the projection onto the positive semidefinite cone. This projection avoids negative eigenvalues in the conservative legitimate-channel covariance approximation.

The spherical uncertainty model is adopted to obtain a tractable robust beamforming update using only the uncertainty radius. This model is conservative because it treats all channel-error directions equally and may overestimate the uncertainty region when the actual estimation error is correlated or direction-dependent. However, it remains useful for a baseline robust design in high-mobility vehicular scenarios, where the exact channel-error covariance may not be reliably available. The projection $\Pi_+(\cdot)$ is therefore used as a numerical safeguard to preserve positive semidefinite covariance behavior after the conservative legitimate-link covariance approximation.

The transmit beamforming vector is then updated using the principal, generalized eigenvector as

$$\mathbf{u}_{\max}^{(k)} = \mathbf{v}_{\max}\left\{ \left(\sigma_E^2 \mathbf{I}_M + P_{\max} \mathbf{R}_E^{(k)}\right)^{-1} \left(\sigma_B^2 \mathbf{I}_M + P_{\max} \mathbf{R}_B^{(k)}\right) \right\}, \tag{44}$$

where $\mathbf{v}_{\max}\{\cdot\}$ denotes the eigenvector corresponding to the largest eigenvalue. The updated beamformer is normalized to satisfy the transmit power constraint as follows:

$$\mathbf{w}^{(k+1)} = \sqrt{P_{\max}} \frac{\mathbf{u}_{\max}^{(k)}}{\left\|\mathbf{u}_{\max}^{(k)}\right\|}. \tag{45}$$

5.2. RIS Phase-Shift Update

For fixed $\mathbf{w}^{(k+1)}$, the RIS phase update is derived by expressing the effective Bob and Eve received signal components as explicit functions of the RIS phase vector. Define

$$\mathbf{z}^{(k+1)} = \widehat{\mathbf{G}}_{AR,\tau} \mathbf{w}^{(k+1)}. \tag{46}$$

The vector $\mathbf{z}^{(k+1)}$ represents the signal incident on the RIS after transmit beamforming and is used in the derivative of the RIS-assisted reflected link. Let

$$d_B = \widehat{\mathbf{h}}_{AB,\tau}^H \mathbf{w}^{(k+1)}, \qquad d_E = \widehat{\mathbf{h}}_{AE,\tau}^H \mathbf{w}^{(k+1)}, \tag{47}$$

and define the RIS-reflected coefficient vectors as

$$\mathbf{q}_B = \widehat{\mathbf{h}}_{RB,\tau}^* \odot \mathbf{z}^{(k+1)}, \qquad \mathbf{q}_E = \widehat{\mathbf{h}}_{RE,\tau}^* \odot \mathbf{z}^{(k+1)}, \tag{48}$$

where $\odot$ denotes the element-wise product. For $\phi_n = e^{j\theta_n}$, the delayed effective scalar channels after beamforming can be written as

$$s_B(\boldsymbol{\phi}) = d_B + \mathbf{q}_B^T \boldsymbol{\phi}, \qquad s_E(\boldsymbol{\phi}) = d_E + \mathbf{q}_E^T \boldsymbol{\phi}. \tag{49}$$

Thus, the role of $\mathbf{z}^{(k+1)}$ is explicit: it links the Alice-RIS channel and the current transmit beamformer to the RIS-phase derivative through $\mathbf{q}_B$ and $\mathbf{q}_E$.

For a given RIS phase vector, define

$$\begin{aligned} a_B(\boldsymbol{\phi}) &= \left[|s_B(\boldsymbol{\phi})| - \varepsilon_B \|\mathbf{w}^{(k+1)}\|_2 \right]_+, \\ a_E(\boldsymbol{\phi}) &= |s_E(\boldsymbol{\phi})| + \varepsilon_E \|\mathbf{w}^{(k+1)}\|_2. \end{aligned} \tag{50}$$

The corresponding robust SNR bounds are

$$\gamma_B^{\mathrm{lb}}(\boldsymbol{\phi}) = \frac{a_B^2(\boldsymbol{\phi})}{\sigma_B^2}, \qquad \gamma_E^{\mathrm{ub}}(\boldsymbol{\phi}) = \frac{a_E^2(\boldsymbol{\phi})}{\sigma_E^2}. \tag{51}$$

For the gradient update, the unclipped robust secrecy surrogate is used as

$$\overline{R}_s^{\mathrm{rob}}(\boldsymbol{\phi}) = \log_2\left(1 + \gamma_B^{\mathrm{lb}}(\boldsymbol{\phi})\right) - \log_2\left(1 + \gamma_E^{\mathrm{ub}}(\boldsymbol{\phi})\right). \tag{52}$$

The final secrecy rate is still evaluated using the non-negative clipping operation, but the smooth surrogate in (52) is used for the local phase-gradient update.

The derivative of the scalar effective channel with respect to the n-th RIS phase is

$$\frac{\partial s_i(\boldsymbol{\phi})}{\partial \theta_n} = j q_{i,n} e^{j\theta_n}, \qquad i \in \{B, E\}. \tag{53}$$

Using the identity

$$\frac{\partial |s_i|}{\partial \theta_n} = \mathrm{Re}\left\{ \frac{s_i^*}{|s_i|} \frac{\partial s_i}{\partial \theta_n} \right\}, \qquad |s_i| > 0, \tag{54}$$

the derivatives of the robust SNR bounds can be written as

$$\frac{\partial \gamma_B^{\mathrm{lb}}}{\partial \theta_n} = \frac{2a_B}{\sigma_B^2} \mathrm{Re}\left\{ \frac{s_B^*}{|s_B|} j q_{B,n} e^{j\theta_n} \right\}, \quad a_B > 0, \tag{55}$$

and

$$\frac{\partial \gamma_E^{\mathrm{ub}}}{\partial \theta_n} = \frac{2a_E}{\sigma_E^2} \mathrm{Re}\left\{ \frac{s_E^*}{|s_E|} j q_{E,n} e^{j\theta_n} \right\}. \tag{56}$$

When $a_B = 0$, the derivative of γ_B^{lb} is set to zero because the lower-bound term is inactive. In numerical implementation, a small positive constant may be added to $|s_i|$ to avoid division by zero.

Applying the chain rule to the difference-of-logarithms objective gives the phase derivative

$$\frac{\partial \overline{R}_s^{\mathrm{rob}}}{\partial \theta_n} = \frac{1}{\ln 2} \left[\frac{1}{1 + \gamma_B^{\mathrm{lb}}} \frac{\partial \gamma_B^{\mathrm{lb}}}{\partial \theta_n} - \frac{1}{1 + \gamma_E^{\mathrm{ub}}} \frac{\partial \gamma_E^{\mathrm{ub}}}{\partial \theta_n} \right]. \tag{57}$$

The continuous phase is then updated using

$$\widetilde{\theta}_n^{(k+1)} = \theta_n^{(k)} + \mu^{(k)} \frac{\partial \overline{R}_s^{\mathrm{rob}}}{\partial \theta_n}, \qquad n = 1, 2, \ldots, N, \tag{58}$$

where $\mu^{(k)}$ is the step size of the k-th iteration. The updated continuous unit-modulus coefficient is

$$\phi_{c,n}^{(k+1)} = e^{j\widetilde{\theta}_n^{(k+1)}}, \qquad n = 1, 2, \ldots, N. \tag{59}$$

To satisfy the finite-resolution RIS hardware constraint, each continuous phase coefficient is first mapped to the nearest element in the discrete phase alphabet:

$$\widetilde{\phi}_{b,n}^{(k+1)} = \arg\min_{\phi \in \mathcal{A}_b} \left| \phi - \phi_{c,n}^{(k+1)} \right|, \qquad n = 1, 2, \ldots, N. \tag{60}$$

Because the nearest-neighbor quantization in (60) may reduce the robust secrecy-rate surrogate, a simple acceptance safeguard is used. Let $\widetilde{\boldsymbol{\phi}}_b^{(k+1)}$ denote the quantized candidate obtained from (60). The candidate is accepted only if

$$\overline{R}_s^{\mathrm{rob}}\left(\widetilde{\boldsymbol{\phi}}_b^{(k+1)} \right) \geq \overline{R}_s^{\mathrm{rob}}\left(\boldsymbol{\phi}_b^{(k)} \right). \tag{61}$$

If this condition is not satisfied, the step size $\mu^{(k)}$ is reduced, and the continuous phase update is repeated. If no improving quantized candidate is found after a preset number of backtracking trials, the previous feasible RIS vector is retained, i.e., $\boldsymbol{\phi}_b^{(k+1)} = \boldsymbol{\phi}_b^{(k)}$. This safeguard prevents a decrease in the retained robust secrecy-rate surrogate during the RIS phase-update step.

The updated RIS phase-shift matrix is then obtained using the accepted quantized phase vector as

$$\boldsymbol{\Theta}_b^{(k+1)} = \mathrm{diag}\left(\boldsymbol{\phi}_b^{(k+1)} \right). \tag{62}$$

5.3. Convergence Criterion and Complexity

After updating $\mathbf{w}^{(k+1)}$ and $\boldsymbol{\Theta}_b^{(k+1)}$, the robust secrecy rate is calculated as

$$R_s^{(k+1)} = R_s^{\mathrm{rob}}\left(\mathbf{w}^{(k+1)}, \boldsymbol{\Theta}_b^{(k+1)} \right). \tag{63}$$

The algorithm stops when

$$\left| R_s^{(k+1)} - R_s^{(k)} \right| \leq \xi, \tag{64}$$

or when the maximum number of iterations $K_{\max}$ is reached.

Due to the non-convex secrecy-rate objective and finite-resolution RIS phase quantization, the proposed alternating

method does not guarantee convergence to the global optimum or to a stationary point of the original mixed-integer problem. The acceptance safeguard in (61) only ensures that the retained quantized RIS phase update does not decrease the evaluated robust secrecy-rate surrogate for the current beamformer. Therefore, convergence in this work refers to numerical stabilization of feasible iterates under the adopted surrogate objective, not to a proof of global optimality.

The channel coherence time can be approximated as

$$T_c \approx \frac{0.423}{f_D}. \tag{65}$$

In high-mobility vehicular links, T_c decreases as the vehicle speed and carrier frequency increase. Therefore, the numerical iteration count reported in this work should be interpreted as algorithmic stabilization behavior under delayed CSI, rather than as a hardware-level guarantee that all iterations can be completed within the instantaneous channel coherence time. Real-time implementation depends on RIS controller latency, channel-estimation delay, feedback signaling, and processing hardware. The proposed model accounts for this practical limitation through the feedback delay τ and the Doppler-dependent uncertainty radius, while real-time low-latency implementation is left as a future extension.

The complete procedure is summarized in Table 4.

TABLE 4. Proposed doppler-aware robust quantized alternating optimization (DA-RQ-AO) algorithm.

Step	Operation
1	Initialize $k=0$, $K_{\max}$, convergence threshold ξ, RIS phase resolution b, transmit beamformer $\mathbf{w}^{(0)}$, and quantized RIS phase matrix $\mathbf{\Theta}_b^{(0)}$.
2	Compute the Doppler correlation coefficient and uncertainty radii using (18) and (29).
3	For fixed $\mathbf{\Theta}_b^{(k)}$, compute the delayed effective channel estimates of Bob and Eve using (40) and (41).
4	Update $\mathbf{w}^{(k+1)}$ using (44) and (45).
5	For fixed $\mathbf{w}^{(k+1)}$, update the continuous RIS phase vector using (58) and (59).
6	Project the continuous RIS phase coefficients onto the b-bit alphabet $\mathcal{A}_b$ using (60). Accept the quantized candidate if it satisfies (61); otherwise, reduce the step size and repeat the RIS phase update. If no improving candidate is found after backtracking, retain the previous feasible RIS vector.
7	Construct $\mathbf{\Theta}_b^{(k+1)}$ using the accepted quantized phase vector in (62) and compute $R_s^{(k+1)}$ using (63).
8	If (64) is satisfied or $k=K_{\max}$, stop; otherwise, set $k=k+1$ and repeat Steps 2–8.
9	Output $\mathbf{w}^\star$, $\mathbf{\Theta}_b^\star$, and $R_s^\star$.

For fixed RIS phases, the beamforming update requires the eigenvalue decomposition of an $M \times M$ matrix, which has complexity $\mathcal{O}(M^3)$. For fixed transmit beamforming, the RIS phase update is dominated by the computation of $\mathbf{z}^{(k+1)} = \widehat{\mathbf{G}}_{AR,\tau}\mathbf{w}^{(k+1)}$, the construction of $\mathbf{q}_B$ and $\mathbf{q}_E$, the phase-gradient evaluation over N RIS elements, and the finite-resolution quantization step. The matrix-vector multiplication for $\mathbf{z}^{(k+1)}$ requires $\mathcal{O}(NM)$ operations; the element-wise construction of $\mathbf{q}_B$ and $\mathbf{q}_E$ requires $\mathcal{O}(N)$ operations; and the evaluation of the phase derivatives for all RIS elements requires $\mathcal{O}(N)$ operations. The nearest-neighbor quantization over the 2^b feasible phase states requires $\mathcal{O}(N2^b)$ operations. If I_{bt} denotes the maximum number of backtracking trials used by the acceptance safeguard, the RIS phase-update complexity is therefore $\mathcal{O}\left(I_{\text{bt}}(NM+N2^b)\right)$.

$$\mathcal{O}\left(K\left(M^3 + I_{\text{bt}}\left(NM+N2^b\right)\right)\right). \tag{66}$$

Since M and b are small in the considered setup, the RIS update scales approximately linearly with the number of RIS elements for each accepted gradient step. This revised complexity expression identifies the dominant operations explicitly and avoids the unsupported $\mathcal{O}(N^2)$ approximation.

6. NUMERICAL RESULTS AND DISCUSSION

The numerical evaluation is performed using a Monte Carlo simulation procedure to account for random channel variations. Unless otherwise stated, each reported average secrecy rate (ASR) and secrecy outage probability (SOP) value is obtained over $L_{\text{MC}} = 1000$ independent channel realizations. For each realization, the direct Alice-Bob and Alice-Eve channels, Alice-RIS channel, and RIS-Bob/RIS-Eve channels are generated using the Rician fading model in (14) with the large-scale path-loss model in (13). The Doppler-dependent temporal correlation coefficient is then computed using (18), and the delayed channel estimates and uncertainty radii are updated according to the imperfect and delayed CSI model described in Section 3. The same set of channel realizations and system parameters is used for all benchmark schemes to ensure a fair comparison.

For each Monte Carlo realization, the transmit beamformer and RIS phase vector are updated until the convergence criterion in (64) is satisfied, or the maximum number of iterations is reached. The ASR is computed as the sample average of the achieved robust secrecy-rate values. The SOP is computed using the empirical outage estimator in (34). For a performance metric X evaluated over L_{MC} trials, the sample mean and the corresponding 95% confidence interval can be expressed as

$$\overline{X} = \frac{1}{L_{\text{MC}}}\sum_{\ell=1}^{L_{\text{MC}}} X_\ell, \quad \overline{X} \pm 1.96\frac{s_X}{\sqrt{L_{\text{MC}}}}, \tag{67}$$

where s_X is the sample standard deviation across independent channel realizations. Plotted curves and summary tables report the Monte Carlo mean values, while the confidence-interval expression is provided to clarify the statistical evaluation procedure and support reproducibility.

This section evaluates the proposed DA-RQ-AO scheme using the system parameters listed in Table 2. The comparison includes four benchmark schemes: no-RIS, random RIS,

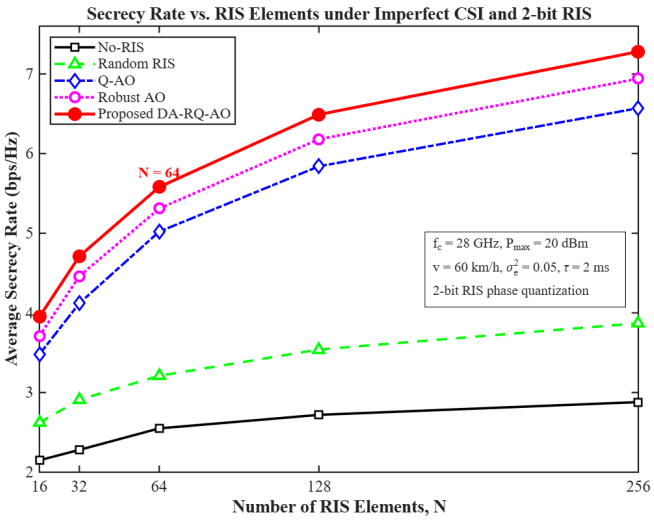

FIGURE 1. Average secrecy rate versus number of RIS elements under imperfect CSI, Doppler mobility, and 2-bit RIS phase quantization.

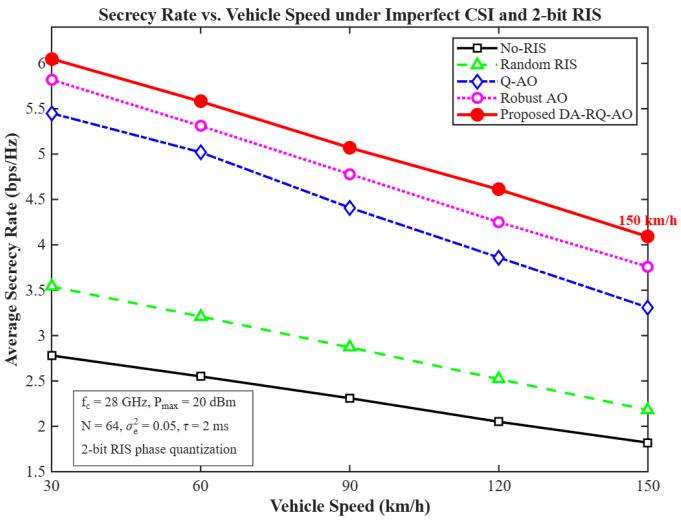

FIGURE 2. Average secrecy rate versus vehicle speed under imperfect CSI, Doppler mobility, and 2-bit RIS phase quantization.

TABLE 5. Benchmark schemes used for performance comparison.

Scheme	Description
No-RIS	Direct transmission without RIS assistance
Random RIS	RIS phases randomly selected from the quantized phase set
Q-AO	Quantized AO without Doppler-aware robust compensation
Robust AO	Imperfect-CSI-aware AO without joint Doppler-aware quantized updating
Proposed DA-RQ-AO	Doppler-aware robust quantized AO under imperfect and delayed CSI

quantized AO (Q-AO), and robust AO, as summarized in Table 5. The no-RIS case considers direct transmission without RIS assistance. The random RIS case uses randomly selected phase shifts from a quantized phase set. Q-AO applies quantized alternating optimization without Doppler-aware robust compensation, whereas robust AO considers imperfect CSI without a joint Doppler-aware quantized update. The selected benchmarks provide an ablation-based comparison under a common system model. No-RIS and random RIS quantify the benefit of RIS deployment and optimized phase control; Q-AO isolates finite-resolution RIS optimization without Doppler-aware robust compensation; and robust AO evaluates imperfect-CSI-aware optimization without the joint Doppler-aware quantized update. SDR-based RIS optimization and artificial-noise-aided secure transmission are relevant state-of-the-art directions; however, direct numerical comparison under the present delayed-CSI, Doppler-aged, passive-Eve uncertainty, and quantized-RIS model would require additional relaxation/randomization, quantization, or artificial-noise covariance design. Therefore, these methods are identified as future comparative extensions, while the present comparison uses equivalent baselines sharing the same channel realizations, power constraint, delayed-CSI setting, and quantized RIS hardware constraint.

To provide a broader comparison beyond ASR alone, Table 6 summarizes the main benchmark schemes under a common default setting. The comparison includes average secrecy rate, secrecy outage probability at $R_{\text{th}} = 3$ bps/Hz, and the approximate number of iterations required to reach a stable secrecy-rate value. This table complements the individual figures by jointly reporting average performance, secure-link reliability, and convergence behavior under the same imperfect-CSI, delayed-CSI, mobility, and 2-bit RIS phase-quantization setting.

The values in Table 6 are evaluated for the common setting $N = 64$, $v = 90$ km/h, $\sigma_e^2 = 0.05$, $\tau = 2$ ms, and 2-bit RIS phase quantization. The ASR values are consistent with the phase-resolution and convergence results, while the SOP values correspond to the outage results at $R_{\text{th}} = 3$ bps/Hz. The table indicates that DA-RQ-AO improves the average secrecy rate and reduces secrecy outage probability compared with the benchmark schemes under the considered default setting. The stable iteration count further indicates that the proposed alternating update reaches a stable feasible solution within a small number of iterations, although this numerical convergence should not be interpreted as a proof of global optimality for the non-convex problem.

6.1. Impact of RIS Elements

Figure 1 shows the average secrecy rate versus the number of RIS elements under imperfect CSI, Doppler mobility, and 2-bit RIS phase quantization. The secrecy rate increases with N because a larger RIS provides more reflecting elements to strengthen the legitimate link and control the leakage toward Eve. At $N = 64$, the proposed DA-RQ-AO scheme obtains 5.58 bps/Hz, whereas the no-RIS and random-RIS schemes obtain 2.55 bps/Hz and 3.21 bps/Hz, respectively. This result indicates the benefit of joint transmit beamforming and Doppler-aware quantized RIS phase control.

TABLE 6. Multi-metric reliability-oriented performance comparison of benchmark schemes under the default simulation setting.

Scheme	ASR	SOP	Stable iter.	Comparison with DA-RQ-AO
No-RIS	2.31	0.66	–	DA-RQ-AO provides 119.5% ASR gain and 72.7% lower SOP.
Random RIS	2.87	0.51	–	DA-RQ-AO provides 76.7% ASR gain and 64.7% lower SOP.
Q-AO	4.42	0.29	≈ 5	DA-RQ-AO provides 14.7% ASR gain and 37.9% lower SOP.
Robust AO	4.78	0.23	≈ 7	DA-RQ-AO provides 6.1% ASR gain and 21.7% lower SOP.
DA-RQ-AO	5.07	0.18	≈ 7	Reference scheme under the default setting.

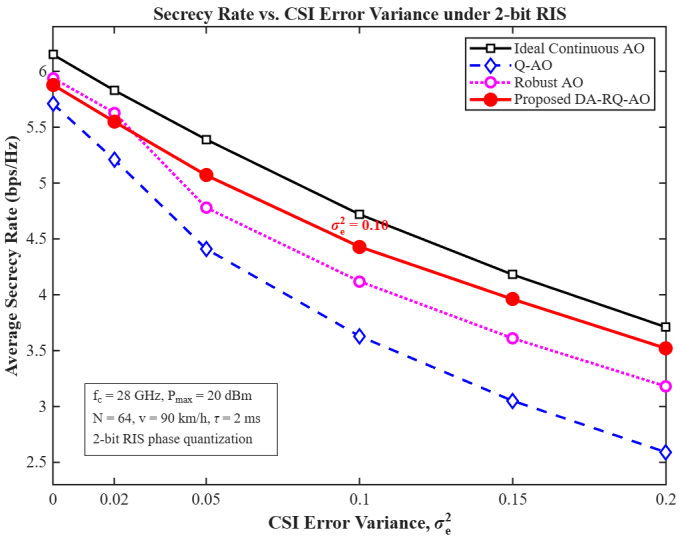

FIGURE 3. Average secrecy rate versus CSI error variance under Doppler mobility and 2-bit RIS phase quantization.

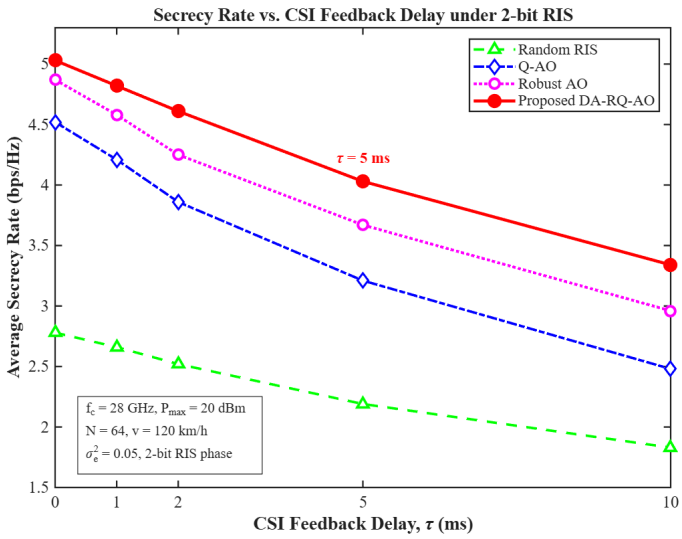

FIGURE 4. Average secrecy rate versus CSI feedback delay under Doppler mobility, imperfect CSI, and 2-bit RIS phase quantization.

6.2. Impact of Vehicle Speed

Figure 2 illustrates the average secrecy rate as a function of the vehicle speed. As the speed increases from 30 km/h to 150 km/h, all schemes experience secrecy-rate degradation because higher mobility increases Doppler-induced channel variation and reduces the reliability of the available CSI. At $v = 150$ km/h, the proposed DA-RQ-AO scheme achieves 4.09 bps/Hz, compared with 3.31 bps/Hz for Q-AO and 3.77 bps/Hz for robust AO. This indicates that Doppler-aware uncertainty updating helps retain a higher secrecy rate under the considered mobility conditions.

6.3. Impact of CSI Error Variance

Figure 3 presents the average secrecy rate versus the CSI error variance. The secrecy rate decreases as σ_e^2 increases because inaccurate CSI causes transmit beamforming mismatch and RIS phase misalignment. At $\sigma_e^2 = 0.10$, the proposed DA-RQ-AO scheme obtains 4.43 bps/Hz, whereas Q-AO obtains 3.63 bps/Hz. This comparison indicates that robust uncertainty modeling is important when the CSI error level increases.

6.4. Impact of CSI Feedback Delay

Figure 4 shows the impact of the CSI feedback delay on the average secrecy rate. Increasing the delay from 0 ms to 10 ms reduces the secrecy rate because the RIS controller updates the phase shifts using outdated channel information. At $\tau = 5$ ms, the proposed DA-RQ-AO scheme achieves 4.03 bps/Hz, compared with approximately 3.20 bps/Hz for Q-AO and 3.67 bps/Hz for robust AO. This result supports the need to consider CSI aging in high-mobility vehicular links.

6.5. Impact of RIS Phase Resolution

Figure 5 compares the secrecy rate under different RIS phase resolutions. The continuous phase case yields the highest secrecy rate and is used as an ideal benchmark. Among the finite-resolution cases, 2-bit phase control incurs only 5.94% loss relative to the continuous-phase benchmark. This indicates that 2-bit RIS phase quantization provides a favorable trade-off between hardware simplicity and secrecy-rate performance.

6.6. Secrecy Outage Probability

Figure 6 plots the secrecy outage probability versus target secrecy rate. As R_{th} increases, the outage probability increases because a higher target secrecy rate is more difficult to satisfy under imperfect and delayed CSI. At $R_{\text{th}} = 3$ bps/Hz, the proposed DA-RQ-AO scheme obtains an SOP of 0.18, compared with 0.66, 0.51, 0.29, and 0.23 for no-RIS, random RIS, Q-AO, and robust AO, respectively. This result shows that the

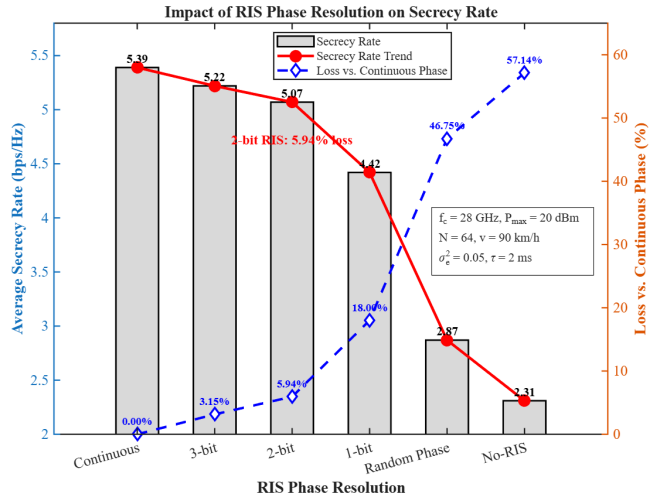

FIGURE 5. Average secrecy rate and performance loss versus RIS phase resolution under Doppler mobility and imperfect CSI.

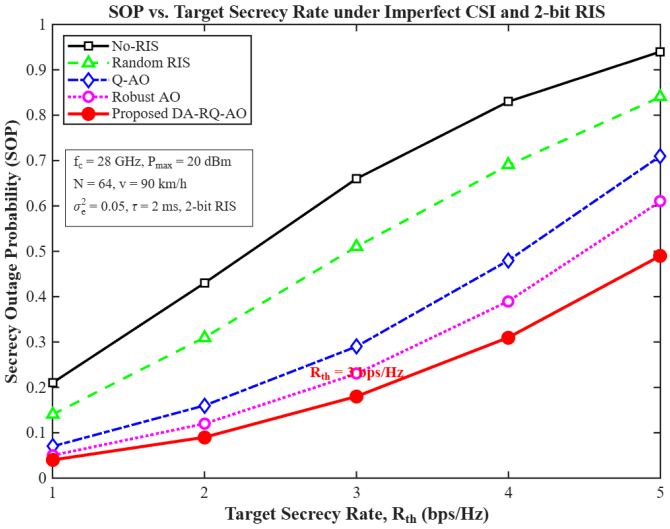

FIGURE 6. Secrecy outage probability versus target secrecy rate under Doppler mobility, imperfect CSI, and 2-bit RIS phase quantization.

proposed design improves secure-link reliability in addition to increasing the average secrecy rate.

6.7. Convergence Analysis

Figure 7 presents the convergence behaviors of the Q-AO, robust AO, and the proposed DA-RQ-AO algorithm. The secrecy rate increases during the first few iterations and then reaches a stable value. The proposed scheme reaches approximately 5.07 bps/Hz within seven iterations, while Q-AO and robust AO stabilize near 4.42 bps/Hz and 4.78 bps/Hz, respectively. This supports the numerical practicality of the alternating update procedure under the considered RIS-assisted vehicular setting.

Consistent with the convergence discussion in Section 5, Fig. 7 shows numerical stabilization of feasible iterates, not global optimality. All schemes are evaluated under the same default settings, with ASR obtained by Monte Carlo averaging and SOP computed using (34).

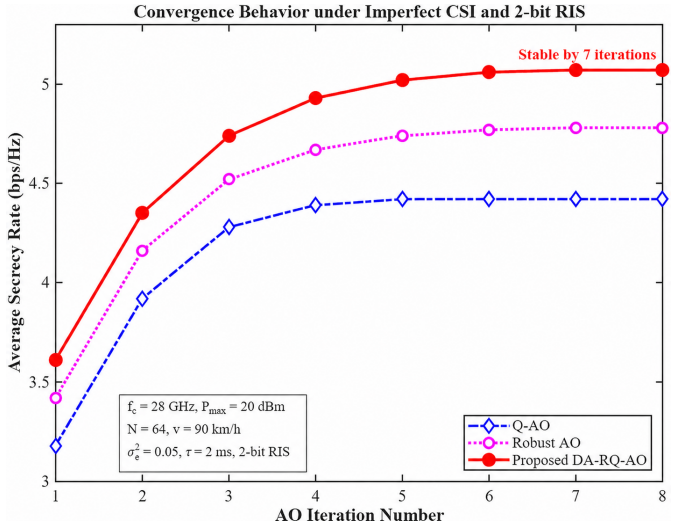

FIGURE 7. Convergence behavior of Q-AO, robust AO, and the proposed DA-RQ-AO algorithm under Doppler mobility, imperfect CSI, and 2-bit RIS phase quantization.

6.8. Overall Performance Summary

The results show that RIS deployment, Doppler-aware robust updating, and low-resolution RIS phase control jointly improve secure vehicular communication. As summarized in Table 6, DA-RQ-AO achieves 5.58 bps/Hz at $N = 64$ and $v = 60$ km/h, reduces SOP at $R_{\text{th}} = 3$ bps/Hz, and shows only 5.94% loss for 2-bit RIS control relative to continuous-phase operation.

7. CONCLUSION

This study has presented a bounded-uncertainty DA-RQ-AO framework for RIS-assisted physical layer security in 6G vehicular networks under imperfect and delayed CSI. The framework jointly considers Doppler-induced channel aging, CSI feedback delay, passive-Eve uncertainty, and finite-resolution RIS phase quantization. A robustness-aware secrecy-rate surrogate was formulated, and an alternating solution was developed using a conservative beamforming update and an explicitly derived RIS phase-gradient update with finite-resolution quantization and an acceptance safeguard.

The numerical results show that DA-RQ-AO improves secrecy performance over no-RIS, random-RIS, Q-AO, and robust AO benchmarks. For $N = 64$ and $v = 60$ km/h, it achieves 5.58 bps/Hz, corresponding to 118.8% and 73.8% gains over no-RIS and random RIS, respectively. The 2-bit RIS case achieves 5.07 bps/Hz with only 5.94% loss relative to continuous-phase control, while the default setting gives an SOP of 0.18 at $R_{\text{th}} = 3$ bps/Hz and numerical stabilization within approximately seven iterations.

Overall, DA-RQ-AO provides a feasible design direction for secure RIS-assisted vehicular communication under mobility, CSI, and hardware constraints. Future work may consider multi-user and multi-eavesdropper settings, active eavesdropping or jamming, ellipsoidal/data-driven uncertainty, real-time RIS control, and network-level validation.

REFERENCES

[1] Noor-A-Rahim, M., Z. Liu, H. Lee, M. O. Khyam, J. He, D. Pesch, K. Moessner, W. Saad, and H. V. Poor, "6G for vehicle-to-everything (V2X) communications: Enabling technologies, challenges, and opportunities," *Proceedings of the IEEE*, Vol. 110, No. 6, 712–734, Jun. 2022.

[2] Mitev, M., A. Chorti, H. V. Poor, and G. P. Fettweis, "What physical layer security can do for 6G security," *IEEE Open Journal of Vehicular Technology*, Vol. 4, 375–388, 2023.

[3] Pan, C., H. Ren, K. Wang, J. F. Kolb, M. Elkashlan, M. Chen, M. D. Renzo, Y. Hao, J. Wang, A. L. Swindlehurst, X. You, and L. Hanzo, "Reconfigurable intelligent surfaces for 6G systems: Principles, applications, and research directions," *IEEE Communications Magazine*, Vol. 59, No. 6, 14–20, Jun. 2021.

[4] Wu, Q. and R. Zhang, "Intelligent reflecting surface enhanced wireless network via joint active and passive beamforming," *IEEE Transactions on Wireless Communications*, Vol. 18, No. 11, 5394–5409, Nov. 2019.

[5] Zhu, Y., B. Mao, and N. Kato, "Intelligent reflecting surface in 6G vehicular communications: A survey," *IEEE Open Journal of Vehicular Technology*, Vol. 3, 266–277, 2022.

[6] Yu, X., D. Xu, Y. Sun, D. W. K. Ng, and R. Schober, "Robust and secure wireless communications via intelligent reflecting surfaces," *IEEE Journal on Selected Areas in Communications*, Vol. 38, No. 11, 2637–2652, Nov. 2020.

[7] Jiang, W., Y. Zhang, J. Wu, W. Feng, and Y. Jin, "Intelligent reflecting surface assisted secure wireless communications with multiple-transmit and multiple-receive antennas," *IEEE Access*, Vol. 8, 86 659–86 673, 2020.

[8] Zhang, Z., C. Zhang, C. Jiang, F. Jia, J. Ge, and F. Gong, "Improving physical layer security for reconfigurable intelligent surface aided NOMA 6G networks," *IEEE Transactions on Vehicular Technology*, Vol. 70, No. 5, 4451–4463, May 2021.

[9] Cao, K., H. Ding, L. Lv, Z. Su, J. Tao, F. Gong, and B. Wang, "Physical-layer security for intelligent-reflecting-surface-aided wireless-powered communication systems," *IEEE Internet of Things Journal*, Vol. 10, No. 20, 18 097–18 110, Oct. 2023.

[10] Shen, M., X. Lei, P. T. Mathiopoulos, and R. Q. Hu, "Robust beamforming design for IRS-aided secure communication systems under complete imperfect CSI," *IEEE Transactions on Vehicular Technology*, Vol. 72, No. 6, 8204–8209, Jun. 2023.

[11] Khalid, W., M. A. U. Rehman, T. V. Chien, Z. Kaleem, H. Lee, and H. Yu, "Reconfigurable intelligent surface for physical layer security in 6G-IoT: Designs, issues, and advances," *IEEE Internet of Things Journal*, Vol. 11, No. 2, 3599–3613, Jan. 2024.

[12] Kaur, R., B. Bansal, S. Majhi, S. Jain, C. Huang, and C. Yuen, "A survey on reconfigurable intelligent surface for physical layer security of next-generation wireless communications," *IEEE Open Journal of Vehicular Technology*, Vol. 5, 172–199, 2024.

[13] Khoshafa, M. H., O. Maraqa, J. M. Moualeu, S. Aboagye, T. M. N. Ngatched, M. H. Ahmed, Y. Gadallah, and M. D. Renzo, "RIS-assisted physical layer security in emerging RF and optical wireless communications systems: A comprehensive survey," *IEEE Communications Surveys & Tutorials*, Vol. 27, No. 4, 2156–2203, 2025.

[14] Makarfi, A. U., K. M. Rabie, O. Kaiwartya, X. Li, and R. Kharel, "Physical layer security in vehicular networks with reconfigurable intelligent surfaces," in *2020 IEEE 91st Vehicular Technology Conference (VTC2020-Spring)*, 1–6, Antwerp, Belgium, May 2020.

[15] Patel, R. and A. Patel, "RIS-assisted physical layer security for vehicular networks in 6G systems," in *2026 International Conference on Electric Power and Renewable Energy (EPREC)*, 1–5, Durg, India, Jan. 2026.

[16] Al-Hilo, A., M. Samir, M. Elhattab, C. Assi, and S. Sharafeddine, "Reconfigurable intelligent surface enabled vehicular communication: Joint user scheduling and passive beamforming," *IEEE Transactions on Vehicular Technology*, Vol. 71, No. 3, 2333–2345, Mar. 2022.

[17] Van Cuong, N., "Robust phase optimization for RIS-assisted SWIPT in 6G networks: A semidefinite relaxation and singular value decomposition-based approach," *Progress In Electromagnetics Research C*, Vol. 157, 259–267, 2025.

[18] 3GPP, "Study on Channel Model for Frequencies from 0.5 to 100 GHz," No. TR 38.901, 3rd Generation Partnership Project (3GPP), Technical Report, version 16.1.0, 2020.